Scientific Research Publishing

Materials Sciences and Applications, 2018, 9, 155-173
http://www.scirp.org/journal/msa
ISSN Online: 2153-1188
ISSN Print: 2153-117X

Ageing Behavior of $LiNi_{0.80}Co_{0.15}Al_{0.05}O_2$ Cathode Based Lithium Ion Cells—Influence of Phase Transition Processes

Christopher Betzin[1,2], Holger Wolfschmidt[1]

[1]Siemens AG, Erlangen, Germany
[2]Friedrich-Alexander-University, Erlangen, Germany
Email: c.betzin@gmx.de

How to cite this paper: Betzin, C. and Wolfschmidt, H. (2018) Ageing Behavior of $LiNi_{0.80}Co_{0.15}Al_{0.05}O_2$ Cathode Based Lithium Ion Cells—Influence of Phase Transition Processes. *Materials Sciences and Applications*, **9**, 155-173.
https://doi.org/10.4236/msa.2018.91011

Received: October 24, 2017
Accepted: January 21, 2018
Published: January 24, 2018

Abstract

In this paper, commercial lithium ion battery cells consisting of graphite based anode and $LiNi_{0.80}Co_{0.15}Al_{0.05}O_2$ (NCA) oxide based cathode were investigated regarding their aging behavior. The capacity loss is dependent on the state of charge (SOC) whereas the battery is operated with partial cycles at defined SOCs. The structural change of the positive electrode material is identified as dominating aging process. Especially grid services such as primary control reserve are of economic interest for battery system operators. In this application, small charge and discharge cycles are the main operation mode. Considering the operation of single battery storage systems in a virtual storage power plant, different states of charges are much more of interest. Thus the battery aging behavior of lithium ion cells with NCA based cathode material with respect to cycling at specific state of charge with small depth of discharge (DOD) is investigated. The results in this paper provide understanding of small DOD cycling at given SOC behavior which is necessary for NCA lifetime prediction in this particular case, especially in virtual storage plant with various storage systems and thus various SOCs for delivery primary reserve the small DOD behavior which has an important impact on efficiency and economy. It is a key finding, which aging mechanisms are essential in order to optimize the cell operation and adapt it to system performance.

Keywords

Cyclic Voltammetry, NCA, Fatigue of LiNCAO, Primary Control Reserve

1. Introduction

Lithium ion batteries play a prominent role for energy storage and are an increa-

singly important part of storage technologies in different sectors [1]-[6]. Based on the reasonable power and energy density of lithium ion batteries, they occupy a huge market share on consumer market like portable electronic devices (e.g. notebooks and tablets) [7]. In the transportation sector, lithium ion storage is at the moment almost indispensable. For full electric vehicles, lithium ion batteries are more important than ever before [8]. Also in hybrid vehicles, lithium ion batteries are used [9]. In combination with grid support, battery vehicles could even supply primary control reserve [10].

But the key role for grid support in an energy market with high share of renewable energy behooves the stationary lithium ion battery energy storage excluded pumped hydro storage [11]. In the case of primary control reserve, lithium ion battery systems are the most promising technology, because of their efficiency and cost structure [12]. One promising use case of lithium ion battery storage systems could be the combination of residential battery systems, to store renewable energy, and the supply of primary control reserve in a virtual storage power plant [13]. For primary control reserve, there are no more full cycles for relevance, but partial cycling will gain in importance. In this case, it is insufficient to know what the impact of decreasing depth of discharge (DOD) is, but even more it is necessary to know in which state of charge region the system behavior could be improved considering aging characteristics of lithium ion cells.

The high efficiency of lithium ion cells compared to other storage technologies like redox flow techniques or lead acid is an advantage. But, it is also cell degradation via aging observed, which is the main disadvantage of lithium ion batteries. An overview of aging mechanisms in literature could be found in [14]. The main aging mechanisms could be divided into two parts, the aging behavior on cycling and the calendric aging effects [15], both effects occur on anode electrodes as well as on cathode electrodes. The most important anode material is graphite. The aging of graphite is dominated by growth of the solid electrolyte interface (SEI) [16] which leads to an increase of internal resistance. It changes the electrode/electrolyte interface via building a solid inorganic electrolyte interface. The main mechanism is the decomposition of organic electrolyte. SEI growth with direct increasing of internal resistance is the main factor of calendric aging. In addition different mechanisms on the cathode side are known for calendric aging. In literature, different materials with different aging behaviors are known, especially deactivation of active material, dissolution of particles and side-reactions of active material [17] [18] [19].

As mentioned before, all active materials suffer under degradation by cycling [20] [21] [22] via mechanical stress and specific chemical depending mechanisms. Based on volumetric change of active material and dissolution and growth of SEI micro, cracks could be observed which are leading to lithium plating [23]. Common used cathode electrode materials are the olivine structured $LiFePO_4$, manganese spinel electrode $LiMn_2O_4$ (LMO) and layered electrodes like $Li_{1+x}(Ni_{1/3}Co_{1/3}Mn_{1/3})_{1-x}O_2$ (NMC). One capacity loss factor of LFP based cathode is dissolution of Fe^{3+} caused due to impurities, which could be generated at sur-

face while cycling [24]. In addition, at the LFP cathode, cracks could be observed by anisotropic effects during coexistence of a Li-rich and a Li-poor phase while cycling [25]. Positive electrodes with $LiMn_2O_4$ (LMO) spinel underlay a degradation caused by local structure effects. The mechanism is the conversion of cubic $LiMn_2O_4$ to a new tetragonal spinel phase with following disintegration in the orthorhombic $LiMn_2O_4$ phase [26]. The layered NMC is very stable by cycling, but structural rearrangements of NMC and change of stochiometry of transition metals leads to capacity loss caused due to higher electrolyte reactivity, which promotes side reactions [27].

In this study the focus is on the cathode material NCA, which is also a layered oxide material and known for long term stability and high energy density. The calendric aging progress is minted on the main effect of a graphite/NCA cell via the growth of SEI and is described in [28]. But changing from calendaric aging to the degradation on cycling aging a strong influence of the cathode is found in [29]. In another investigation on NCA based lithium ion batteries increased current rates with high DOD lead to a rapid degradation of the active material caused by micro cracks on the surface [30]. Especially this finding will be conducted in the following discussion for the findings obtained here. In addition an inactive state of Ni^{3+} and Ni^{2+} is observed in [31] with oxygen loss of the active material. This leads to disabled lithium for intercalation and deintercalation, resulting in changes of the cell behavior at exactly given potentials. As an important effect in NCA materials a phase transition is known with a crystal structure change between monoclinic to hexagonal [32]. This transition is at a fixed potential which can directly correlated with the finding obtained in the results part and discussed later on.

2. Measurements

In this section the measurement procedures are presented. The investigated cells are commercial 45 Ah lithium ion battery round cells with a graphite based anode and a $LiNi_{0.80}Co_{0.15}Al_{0.05}O_2$ (NCA) based cathode material with organic electrolyte and hexafluorophosphate lithium salt $LiPF_6$. The procedure is started with a galvanostatic measurement for cycling with small depth of discharges at specific state of charge (SOC) and subsequent periodic capacity determination to investigate capacity progress. After every 1000^{th} partial cycle an electrochemical impedance spectroscopy for the investigation of impedance development, in order to interpret ohmic, charge transfer and diffusion behavior is carried out. The third part of measurement procedure is the cyclic voltammetry (CV). Based on CV the mechanism of different degradation behavior is discussed. The potentio dynamic measurement allows conclusions about electrochemical behavior concerning the kinetics and physical processes on the electrodes [33].

2.1. Cycling Tests

The cycle tests are executed with a battery test system Basytec XCTS. In order to control the ambient temperature a climate chamber CTS T-40/350 is used. The

SOC is adjusted via Ah counter with an accuracy of ±0.2%. In this study two average states of charge are considered. The first state of charge is at 30% SOC with an initial open circuit voltage of 3.53 V and the second cycle test belongs to the state of charge 70% (OCV of 3.75 V). For each cycle test two cells are considered and the current rate is C/3.

After every 1000th partial cycle with a DOD of 10% executed via an Ah-counter a characterization cycle is carried out. That characterization cycle is done for capacity determination and readjusting the SOC, which was not necessary during the whole testing time. In order to determine the capacity loss two discharge capacities are specified. After the common CC-CV charge cycle with CV potential of 4.0 V and the abort criterion of C/20, a discharge with CC of C/3 like charging is done. Subsequently a constant voltage phase at 2.7 V with the same abort criterion like charging is carried out. Table 1 shows the comparison of the cycling conditions.

2.2. Electrochemical Impedance Spectroscopy (EIS)

After each 1000th cycle a galvanostatic electrochemical impedance spectroscopy (EIS) is carried out to interpret the capacity loss behavior. The impedance spectroscopy is done via multi-channel galvanostat/potentiostat EC-Lab Biologic VMP3 and a current Booster VMP3 B-10. The ambient temperature is controlled by the climate chamber Binder KB53. The impedance spectroscopy is used to determine internal resistance and interfacial capacitance of cell. The basic of this measurement is by reference an AC source to determine the impedance depending on frequency by varying it. The measurement allows interpreting equivalent resistance and interfacial capacitance values by means of correlation to electrode interfacial phenomena [34]. In this study the carried out bandwith of frequency is 6 kHz up to 50 mHz with 36 points per decade in logarithm spacing. Per each frequency an average of two measurement points is carried out. The galvanostatic impedance mode is carried out with an amplitude of 1 A.

Table 1. Cycling initial condition (voltage limit) at 25˚C ambient temperature with 10% DOD at SOC 30% and 70%.

	30% SOC	70% SOC
OCV	3.53 V	3.75 V
Charge (C/3) to	3.62 V	3.85 V
Discharge (C/3) to	3.44 V	3.65 V
	1000 partial cycles with 10% DOD	
Charge CC (C/3) to	4.0 V	
Charge CV	4.0 V (C/20)	
Discharge CC (C/3) to	2.7 V	
Discharge CV	2.7 V (C/20)	
	Capacity determination	

2.3. Cyclic Voltammetry (CV)

The potentio dynamic measurement cyclic voltammetry is realized by multi-channel galvanostat/potentiostat EC-Lab Biologic VMP3 and current Booster VMP3 B-10. The different ambient temperatures between 10˚C and 40˚C are controlled by a climate chamber Binder KB53. The constant potential scan rate is varied between 0.020 $mV \cdot s^{-1}$ and 0.022 $mV \cdot s^{-1}$ in order to get physical dependency. This measurement is carried out to evaluate electrochemical process at electrodes surfaces [35].

In order to get an impression which impacts the aging process on potentio dynamic behavior has, in **Figure 1** cyclic voltammograms of a pristine and fatigue cell are shown. In order to determine changes in electrochemical mechanism processes while aging, cyclic voltammetry is carried out to correlate aging phenomena with electrochemical processes, which are known in literature [36].

3. Results

The first results are shown in **Figure 2**. Two cells were cycled at 70% SOC with a DOD of 10% and a current of C/3 with an ambient temperature of 25˚C and two cells were cycled at 30% SOC by the same conditions. In **Figure 2(a)** the capacity was determined with common CC-discharge mode. In **Figure 2(b)** the capacity was determined with CC-CV-discharge mode shown at left y-axes and the averaged 1 kHz resistance determined from both cells per each test at 50% SOC is shown at the right y-axes.

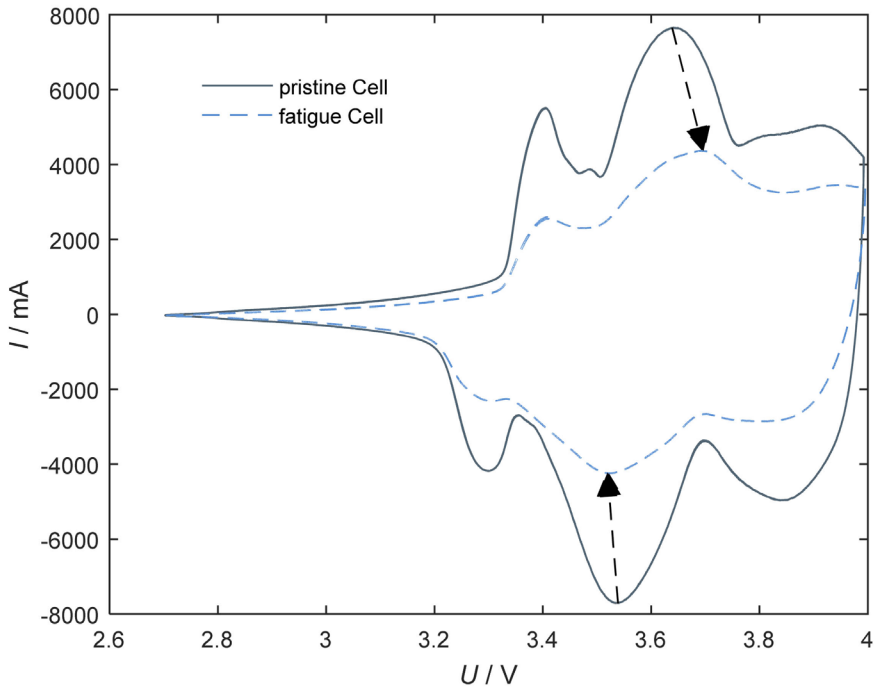

Figure 1. Cyclic voltammatry of a commercial lithium ion battery cell with NCA-based cathode electrode of a pristine cell (black line) and a fatigued cell (light blue dashed line) with a potential scan rate of 0.020 $mV \cdot s^{-1}$ at ambient temperature of 25˚C.

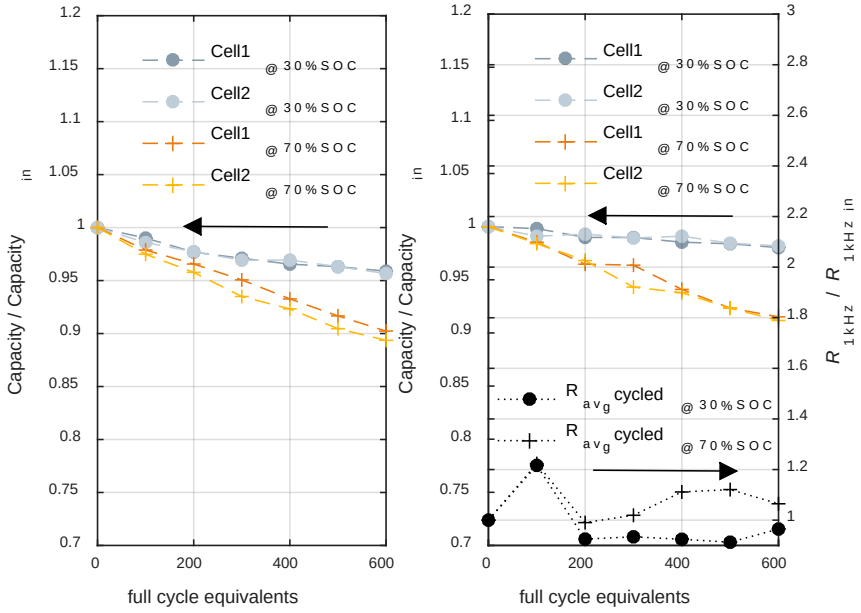

Figure 2. Capacity fade of cycle tests at 25˚C ambient temperature (a) determined with CC-discharge protocol for each test with two cells, grey dots cycled at 30% SOC and yellow crosses cycled at 70% SOC; (b) Capacity progress determination via CC-CV-discharge protocol with two cells for each test with grey dots cycled at 30% SOC and yellow crosses cycled at 70% SOC with averaged 1 kHz resistance determined from both cells per each test at 50% SOC with same marker as capacity measurement.

The capacity loss shown in those figures allows assigning a state of charge depending degradation of NCA cathode based lithium ion cells with graphite based anodes. Discharge only with a constant current phase at the end correlates in general directly with the growth of resistance. In order to validate the reversible amount of capacity loss, caused due to lithium binding the capacity loss by CV discharge is considered. The additional CV procedure allows the interpretation of approximately current independent ($I \rightarrow 0$) lithium loss, caused due to lithium binding which doesn't inevitably directly correlate with growth in internal resistance.

Considering the subplot a) after 600 full cycle equivalents a quantitative higher capacity loss with respect to CC discharge mode by cycling at 70% SOC compared to cycling at 30% SOC is observed. Whereas cycling at 30% SOC leads only to a loss of about 2% of the initial capacity after 600th full cycle equivalents, cycling at 70% SOC leads under the same condition to 10% capacity loss. Both redundant cells show for each cycle test the same behavior.

The aging dependent capacity loss of these both cycling tests can be described by a linear or square root full cycle equivalent dependent function and is detailed discussed in [37].

Considering the subplot **Figure 2(b)** also a difference of capacity losses between cycling at 70% SOC compared to cycling at 30% SOC is observed, which is seen on the left y-axis. The capacity loss which is observed by CC-CV-mode ad-

mits an interpretation of irreversible loss of lithium capacity. For both cycle test conditions also an irreversible capacity loss of lithium could be observed. In particular for cycling at 70% SOC the irreversible loss is dominating. The difference between CC-mode in subplot **Figure 2(a)** and CC-CV mode in subplot **Figure 2(b)** capacity leads to the conclusion, that cycling at 30% has less impact on internal resistance growth and on irreversible binding of lithium compared to 70% SOC.

Considering the right y-axis in subplot **Figure 2(b)** the internal resistance progress at 1 kHz and 50% SOC is directly correlated with the ohmic resistance [38], is illustrated. The internal resistance is a slightly increasing cycling at 70% SOC leads to higher resistance compared to cycling at 30% SOC, but this result is not sufficient to explain the high rise of capacity loss.

In order to interpret the capacity fade results an EIS is carried out. The Nyquist plot is illustrated to visualize the complex and real part of impedance [39]. The impedance spectroscopy is executed at 70% SOC and 30% SOC for each cell independent on cycle test.

In **Figure 3** the results of electrochemical impedance spectroscopy after 6000 partial cycle test at 70% SOC and 30% SOC from 6 kHz up to 50 mHz with current amplitude of 1 A and 36 points per decade are shown. In **Figure 3(a)** the results of EIS at 70% SOC where the dark grey dots after cycling at 70% SOC and the light blue dots after cycling at 30% SOC are illustrated.

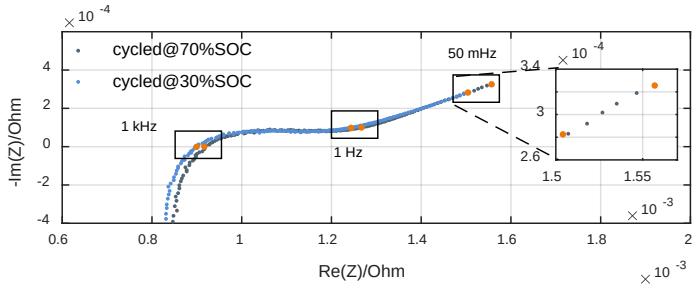

(a)

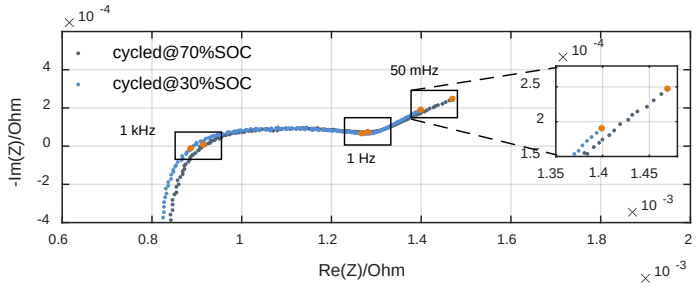

(b)

Figure 3. Electrochemical impedance spectroscopy after 6000 partial cycle at 70% SOC and 30% SOC from 6 kHz up to 50 mHz with current amplitude of 1 A and 36 points per decade with logarithm spacing. (a) Two Nyquist plots at 70% SOC with cycled cell at 70% SOC (grey dots) and cycled cell at 30% SOC (light blue dots); (b) Two Nyquist plots at 30% SOC with cycled cell at 70% SOC (grey dots) and cycled cell at 30% SOC (light blue dots).

In Figure 3(b) the results of EIS at 30% SOC under otherwise identical conditions as in subplot Figure 3(a) are shown.

Applying electrochemical impedance spectroscopy at lithium ion battery cells, three major frequency subdivisions are relevant. The first section deals with frequencies higher than 1 kHz, where inductive phenomena occur, which is not detailed investigated in this study. The intersection with the x-axis which is approximately at 1 kHz in the Nyquist plot is one important point for investigation. At this point no relevant imaginary term of impedance is observed; always the real part of impedance is decisive, which represents the ohmic resistance. The second subdivision in Nyquist plot is the medium frequency range. The frequencies are between 1 kHz and approximately 1 Hz. In this frequency range the electrochemical charge transfer processes with double-layer charging occur. At lower frequency as approximately 1 Hz the diffusion limiting process is observed [40].

Comparing the results of EIS at 70% SOC by cycling around 70% SOC a higher increase of ohmic resistance (intersection axis of abscissa) is seen compared to the cell cycled at 30% SOC. Also the ohmic resistance at 30% SOC is by cycling at 70% SOC compared to cycling at 30% SOC higher. Those results match to the observed behavior before. In this case no correlation between SOC and ohmic resistance is determined.

The resistance between intersection axis of abscissa and minimum at lower frequencies [41] strongly depends on the charge transfer in a battery cell. As in the Nyquist plot illustrated, no significant change in charge transfer could be observed. Neither differences at cycling at 30% SOC, nor cycling at 70% SOC in EIS at 30% SOC and 70% SOC are shown. Based on these results no charge transfer inhabitation is found.

For lower frequencies the diffusion process is the most important phenomena [42]. The resistance part could be deduced at the point with highest real and complex part of impedance in the Nyquist plot [43]. First it could be observed that the diffusion resistance belongs is higher at 70% SOC. In addition cycling at 70% SOC leads also in EIS at 30% SOC and 70% SOC to higher value in impedance. The real term by cycling at 70% SOC of impedance as well as the imaginary term of impedance has larger values compared to cycling at 30% SOC.

According to literature at lower frequencies, diffusion limiting processes are the dominant phenomena in lithium ion battery cells. In order to describe those processes the Warburg impedance is used in general [44] [45].

In Equation (1) the Warburg impedance Z_W is shown, where ω the frequency, $R_W(\omega)$ the frequency depending real term of impedance, R the ideal gas constant, T the temperature, i the imaginary unit, F the faraday constant and c^0 the concentration, n the amount of transferred electrons and D the diffusion coefficient is.

$$Z_W = R_W(\omega) + \frac{2\sqrt{\omega}RT}{i\omega n^2 F^2 c^0 \sqrt{2D}} \quad (1)$$

Considering the equation of Warburg impedance in connection with the previous results the diffusion coefficient is of interest. The cells cycled at 70% SOC show at impedance spectroscopy at lower frequencies especially at 0.05 Hz both in real part of impedance as well as in the imaginary part higher values compared to the cells cycled at 30% SOC. With regard to Warburg impedance, where the frequency at 50 mHz is fixed and the temperature is constant, no changes in parameters are possible except the diffusion coefficient. The higher impedance values are possible if the diffusion coefficient decreases caused due changes in the material. In this case the aging mechanism with respect to impedance results is directly correlated with diffusion limiting processes.

Based on cyclic voltammetry the oxidation and reduction process could be observed. In this study the change of oxidation and reduction processes of NCA based lithium ion cells with graphite anode are shown. The CV's in **Figure 4** show the differences between a pristine cell and two cycled cells, cycled at 30% SOC and 70% SOC, while charge and discharge processes. The first process between charge and discharge is around 3.3 V and 3.4 V, the peaks belong to the graphite anode [46]. Considering the pristine cyclic voltammogram the two peaks between 3.53 for lithium intercalation in NCA and 3.63 from deintercalation show the primary electrode process. The cycled cell at 70% SOC shows a significant changed CV compared to the cycled cell at 30% after 500 full cycle equivalents. Considering the CV of the pristine cell compared to the cell cycled at 30% SOC no remarkable differences are seen. First of all the current intensity of the main peak pair for reduction and oxidation process between cycled

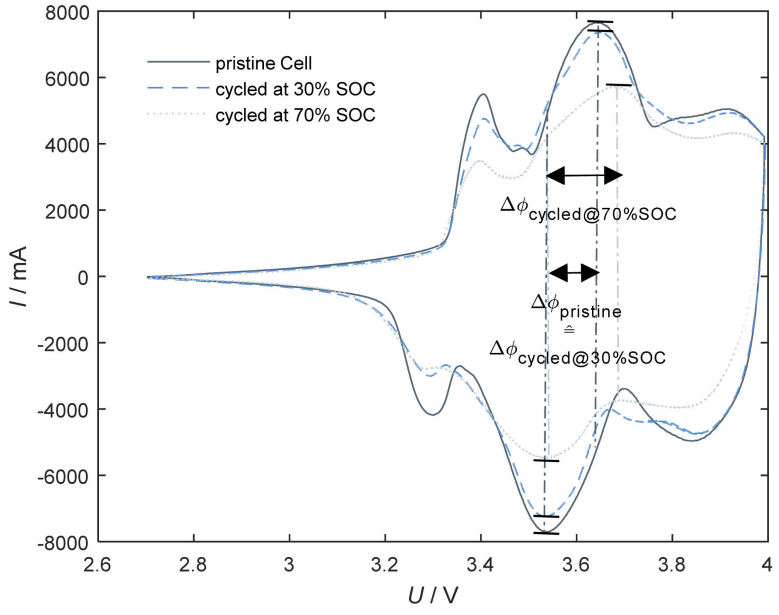

Figure 4. Cyclic voltammograms at 25˚C ambient temperature with a constant potential scan rate of 0.020 $mV \cdot s^{-1}$ of a commercial pristine cell with NCA-based cathode (dark grey line) and one cell after 5000 partial cycles with 10% DOD at averaged 30% SOC (light blue dashed line) and one cycled cell around averaged 70% SOC (light grey dotted line) including potential shift $\Delta\varphi$ and distinctive oxidation and reduction peak points.

cell at 70% SOC compared to cycled cell at 30% SOC is decreased by 2000 mA, due to different aging processes. Beside the reduction of current intensity while discharge and charge, especially the overpotential of lithium deintercalation at the NCA cathode is increased by 45 mV. Considering the potential shift $\Delta\varphi$ between all three cells a further difference in aging behavior is observed. Whereas the cell cycled at 30% SOC compared to the pristine cell no shift is shown, a potential shift $\Delta\varphi$ by cycling at 70% SOC is indicated in Figure 4. Thus, aging behavior regarding cycling with small DOD at different SOC causes a phase change in NCA material.

In Figure 5 cyclic voltammetry at two different temperatures in order to determine temperature depending electrochemical processes is carried out. The scan rate of 0.020 $mV \cdot s^{-1}$ for the positive and the negative sweep is constant. For each pair of peaks a potential shift $\Delta\varphi$ is observed, especially the lithiation and delithiation is of interest. At higher temperature (40˚C) less potential difference compared to low temperature (10˚C) is detected. According to literature a diffusion process is the main inhibiting process, in addition the charge transfers play no mayor role in this case [47]. The main mechanism of this electrochemical process is diffusion limited. But one additional mechanism is observed. The ratio of current density j^+/j^- is not constant, in this case a temperature depending change in charge transfer occurs. The reduction of current density depending on less temperature while lithinate NCA-based material is higher compared to the reduction of delithiation current density. Current density in general depends on

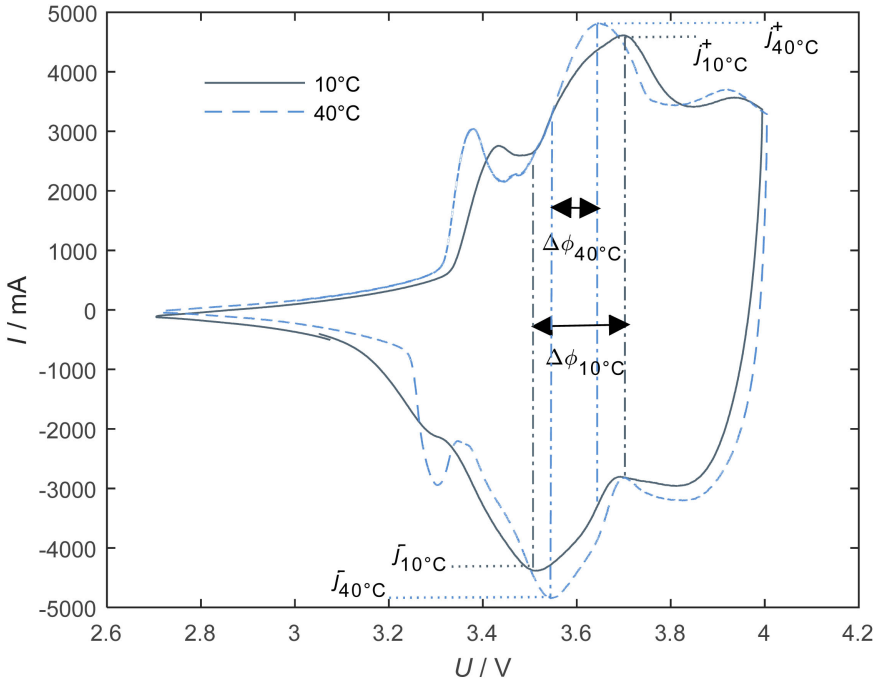

Figure 5. Cyclic voltammograms of a commercial Li NCA cell after partial cycles with 10% DOD at averaged 70% SOC with a constant potential scan rate of 0.020 $mV \cdot s^{-1}$ at 10˚C ambient temperature (dark gray line) and at 40˚C ambient temperature (light blue dashed line) including potential shift $\Delta\varphi$ and current density peaks j.

temperature. Decreasing temperature leads to decreasing current, because electrochemical processes are kinetic depending processes, which is seen in Equation (2) where j, j_0 are the current densities with $\Delta^r G$ the free reaction enthalpy, R the ideal gas constant and T the temperature.

$$j = j_0 e^{\left(\frac{\Delta^r G}{RT}\right)} \tag{2}$$

Especially for electrochemical processes the Butler-Volmer equation is used, where F is the Faraday constant, α is the transfer coefficient and η is the overpotential.

$$j = j_0 \left(e^{\left(-\frac{\alpha nF}{RT}\eta\right)} - e^{\left(-\frac{(1-\alpha)nF}{RT}\eta\right)} \right) \tag{3}$$

Oxidation and reduction underlay different mechanism; a variation and an asymmetrical change of current density are shown. In this case lithiation while changing the crystal structure is inhibited. During this change the lattice parameter varies. According to literature the oxide delithiation process which occurs while charging the cell results in a decrease lattice occupancy fraction [47]. In order to confirm the previous results the variation of potential scan rate is carried out.

One important parameter for interpreting CV is the potential scan rate. In Figure 6 two CV's with different potential scan rates 0.020 $mV \cdot s^{-1}$ and 0.022 $mV \cdot s^{-1}$ of the aged cell cycled at 70% are shown. In this case the current intensity

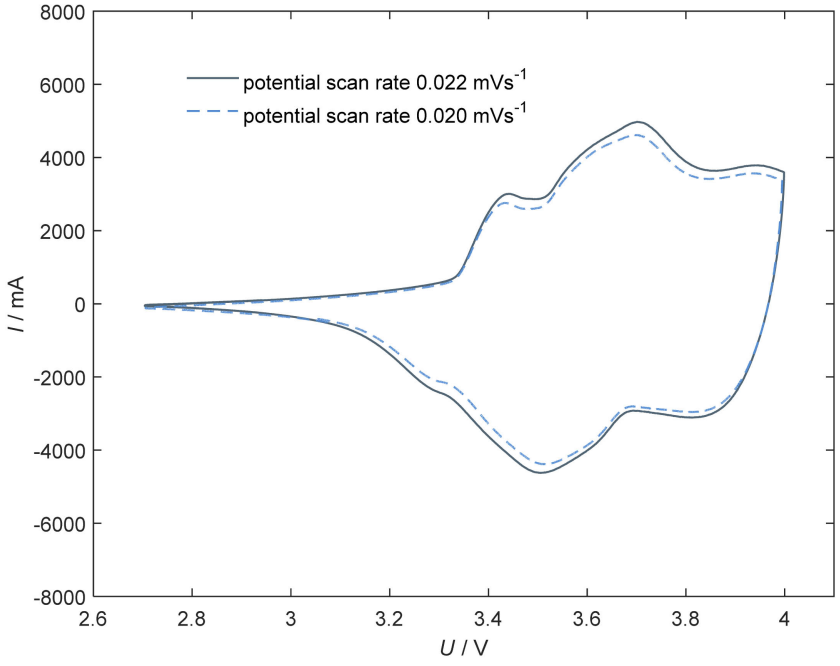

Figure 6. Cyclic voltammograms of a commercial NCA cathode based cell after partial cycles with 10% DOD at averaged 70% SOC at 10˚C ambient temperature with a constant potential scan rate of 0.022 $mV \cdot s^{-1}$ (dark gray line) and a constant potential scan rate of 0.020 $mV \cdot s^{-1}$ (light blue dashed line).

decreases with lower potential scan rates. Also the difference between absolute current for oxidation and reduction is constant. But one important result is the fixed overpotential between oxidation to reduction peak. If a reaction with inhibited charge transfer as main mechanism exists a difference between overpotential at different scan rates will occur. If a diffusion limited process is the main mechanism no change between overpotential will be observed. In this case the behavior hint to diffusion limited process.

In general the mechanisms of cyclic voltammetry are shown in **Figures 4-6**. For an aged cell at **Figure 5** a potential difference between lithiation and delithiation state at cycling around 70% is observed. The conclusion is a diffusion limitation in lithiation of NCA which is a conclusion of irreversible loss of lithium while changing crystal structure, which leads to change in lattice parameter [48] and changes in addition the state of nickel ions. In this case nickel ions will be inactive during change and the lithium intercalated in the NCA material is not completely able to delithinate, which leads to an additional barrier regarding change in order of nickel with potential change. In addition to this process the current density while discharge and therefore lithiation of NCA decreases.

According to literature [36], an overpotential $\Delta\varphi$ should be observed, if an electrochemical charge transfer is inhibited. This is not seen in **Figure 6**, no increase of $\Delta\varphi$ is observed. In this case the main mechanism is a diffusion limited reaction. Considering **Figure 5** it apparently supports that theory. If temperature is changed, a high difference between potential of reduction and oxidation is determined, but also a change of current density ratio with limitation to lithiation of NCA happens. In this case a diffusion depending limitation could be observed with additional change in reaction mechanism, which is temperature depending. In this case the lattice parameter change, which is known in literature [48] playing a key role limiting the diffusion limitation and leading to irreversible losses of lithium.

One additional important investigation during aging processes is temperature behavior. As mentioned before, change in crystal structure is one important mechanism of aging a NCA-based Li-ion cell by cycling with small DOD. The phase change leads to a variation in lattice parameter and changes the order of the system. In this case the entropy of system is changed. The entropic effect has an impact on aging behavior of NCA-cathodes, because entropy change of solid materials leads in general to structural stresses. In order to determine entropic effects the change in temperature is the key factor [49]. The change in entropy in general could be positive or negative, which results in positive or negative temperature gradients in the cell.

Considering **Figure 7(c)** at charging and discharging process the temperature development shows a non linearity behavior. It is known that increased temperature gradients at boundary voltage areas occur due diffusion limitation [50].

Around 3.6 V to 3.8 V while charge process and 3.6 V to 3.5 V while discharge process entropic effects of NCA could be observed. In this area a change of crystal structure leads to an entropic effect. Based on internal resistance at current

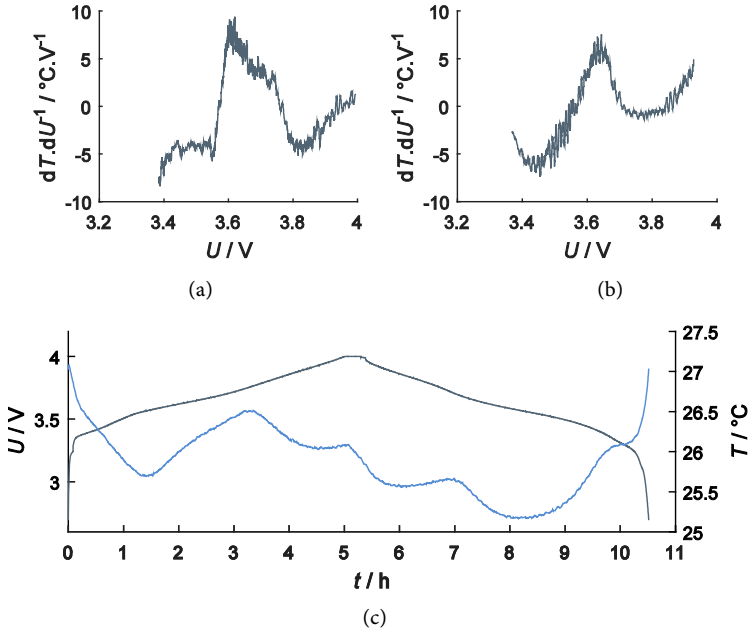

Figure 7. (a) Differential temperature voltammetry while charge at 25˚C ambient temperature; (b) Differential temperature voltammetry while discharge at 25˚C ambient temperature; (c) Temperature behavior of a commercial LiNCA cell while a standard CC-CV charge and CC-discharge cycle with C/5 and ambient temperature at 25˚C.

flow temperature arises with ohmic losses. Only entropic losses could change the behavior in electrochemical cells. In this case the phase transition of NCA could be the reason. Cycling between 3.65 V and 3.85 V leads to a higher average temperature in contrast to cycling between 3.44 V and 3.62 V. In this case two main factors for accelerated aging by cycling around 70% SOC are determined.

The derivative of voltage above the derivative of temperature could be used to describe the reaction entropy $\Delta^{r}S$ [51].

$$\frac{\mathrm{d}T}{\mathrm{d}U}=\frac{nF}{\Delta^{r}S} \tag{4}$$

In order to determine the temperature development due to entropic effects the differential temperature voltammetry [52] is carried out.

$$DTV=\frac{\frac{\mathrm{d}T}{\mathrm{d}t}}{\frac{\mathrm{d}U}{\mathrm{d}t}}=\frac{\mathrm{d}T}{\mathrm{d}U} \tag{5}$$

Shown in **Figure 7(a)** and **Figure 7(b)** the highest entropic effect of temperature evaluation occurs between 3.6 and 3.7 V. Considering cyclic voltammetry that area is congruent with the maximum peak of phase transition. But the gradients by cycling at 70% lead to higher temperature development and entropic effects caused by transition and lead to higher mechanical stress. Considering the peak in **Figure 7(a)** it is also shown, that the charging process with respect to phase transition leads to a positive temperature gradient. The change in entropy regarding phase transition while charge process is negative caused due to posi-

tive temperature evolution. The negative change in entropy could be explained by reduction of lattice parameter. Considering the peak in **Figure 7(b)** it is shown, that the discharging process with respect to phase transition leads also to a positive temperature gradient, but the negative voltage development leads to a decrease in absolute temperature. The change in entropy regarding phase transition while discharge process is positive caused due to negative temperature evolution. The positive change in entropy could be explained by increase of lattice parameter.

4. Discussion

It is known in literature, that the cathode material is the dominant part for aging of NCA-cathode based with graphite anode based battery cells [29]. Also it is well studied, that micro cracks in cathode material are one of the main degradation mechanism [48]. In those studies high current rates or high depths of discharge are the typical measurement conditions [30].

Regarding the capacity fading different results are obtained with respect to cycling at 70% SOC compared to cycling at 30% SOC with small DOD. The detailed capacity progress with respect to d aging at 70% SOC is investigated. In literature a phase transition in the region of 70% SOC is known, this is a change from monoclinic to hexagonal structure [32] where lattice parameter changes. Based on impedance spectroscopy the diffusion behavior is determined as main inhibiting processes. Moreover, cyclic voltammetry is carried out to identify the impact of phase transition with respect to potentio dynamic behavior caused due to the different aging processes. This is a direct correlation between phase transition and aging process. By varying the parameters potential scan rate and the temperature also a diffusion limitation is determined. According to literature an inactive state of Ni^{3+} and Ni^{2+} with oxygen loss of active material is known [31], which disabled lithium intercalation and deintercalation. With respect to the received results the diffusion limitation regarding the phase transition is an aging mechanism for cycling with small depth of discharges. Additionally, the differential thermal voltammetry is carried out to determine the effect of entropy with respect to the temperature influence. The results show a direct impact of entropy caused due to the temperature behavior regarding the change in crystal structure. This entropy depending temperature profile has an additional impact on aging processes.

In order to underpin the results received in this study, the anode material should be mentioned. According to literature the graphite anode combined with NCA based cathode is not the main aging factor [28]. But one mechanism with respect to cell aging of graphite/NCA belonging to anode side is discussed in literature [53]. Particular at 3.7 V and higher potential lithium plating is observed. In this region a lower charge transfer coefficient is expected. But also here high current and particularly deep temperatures are necessary [54]. In both studies the high current rates and deep temperatures are determined as main factor for lithium platting. Those measurement conditions are excluded in this study.

5. Conclusions

The study was performed with a graphite anode based lithium ion battery combined with a NCA oxide base cathode. A strong dependency between cycling with small DOD at different SOC was observed. If cycling around 30% SOC with 10% DOD is carried out, a much better life time performance could be reached in contrast to cycling around 70% SOC. The NCA based lithium ion battery cycling around 30% SOC shows after 600 full cycle equivalents only a degradation of about 2%, whereas cycling around 70% SOC leads to a capacity decrease of 10%. Considering the results, the difference is a starting point for optimization, in order to enhance battery system lifetime. This cycling behavior knowledge is necessary for NCA lifetime prediction, especially in virtual storage plant for delivering primary reserve and has an important impact on efficiency and economy, caused on the possibility to deal with different system states. It is important to know, which aging mechanisms are essential in order to optimize the cell behavior and adapt it to system performance.

Furthermore, the behavior of capacity loss could be described by cyclic voltammetry in detail. We could correlate different effects to the physico chemical effects like phase transitions. It could be shown, that fatigued NCA lithium ion battery cells cycled with small DOD depend strongly on state of charge and so on phase transition. Also the impact of reversible heat and the entropic effect were interpreted. It was shown, that the diffusion of the electrochemical system is limited. In addition an electrochemical discharge inhibition occurs while degradation progress. According to literature and in post mortem analyses, the disorientation of Ni [32] could be observed and confirmed.

Also impedance analysis via spectroscopy was carried out and confirmed the results. A higher temperature in average by cycling around 70% state of charge compared to cycling around 30% SOC was found. An additional increase of internal resistance at higher frequencies which correlate with growth in SEI and also at lower frequencies which correlate with diffusion processes could be determined.

In future, additionally to existing results from NCA aging behavior, other state of charges (SOC) will be investigated to support the degradation theory and optimize the aging depending use of decentralized and distributed battery system for supplying primary control reserve in a virtual storage plant. Furthermore, the ambient temperature of cycling will be changed to see the impact of temperature correlation to the phase transition. In following investigation, additional cathode electrode chemistry will be investigated to encourage the results.

Acknowledgements

The authors thank Caterva GmbH for helpful discussions regarding the operation of the virtual energy storage plant with decentralized battery storage systems. The work was partly financial supported by Public Research Program IET-1401-0004.

References

[1] International Energy Agency (2015) Energy Technology Perspectives 2015. Paris.

[2] International Energy Agency (2015) World Energy Outlook 2015. Paris.

[3] Thrän, D., Dotzauer, M., Lenz, V., Liebetrau, J. and Ortwein, A. (2015) Flexible Bioenergy Supply for balancing Fluctuating Renewables in the Heat and Power Sector—A Review of Technologies and Concepts. *Energy, Sustainability and Society*, **5**, 1-15. https://doi.org/10.1186/s13705-015-0062-8

[4] Price, A. (2015) Storage Technology and Future Developments. *Energy Storage: What's Next for the Grid*? 1-23. https://doi.org/10.1049/ic.2015.0074

[5] Landry, M. and Gagnon, Y. (2015) Energy Storage: Technology Applications and Policy Options. *Energy Procedia*, **79**, 315-320. https://doi.org/10.1016/j.egypro.2015.11.494

[6] Pillot, C. (2012) The Worldwide Battery Market 2011-2025. Batteries 2012, Nice.

[7] Markets and Markets (2014) Portable Battery Pack Market by Capacity Range, Product Type (Smartphone, Tablet, Portable Devices and Others), Technology (Li-Ion, Nickel Metal Hydride, Li-Polymer, and Nickel Cadmium) & Geography—Global Forecast to 2014-2020.

[8] He, J.J., Hu, K.-W. and Liaw, C.-M. (2015) On a Battery/Supercapacitor Powered SRM Drive for EV with Integrated On-Board Charger. *IEEE International Conference on Industrial Technology* (*ICIT*), March 17-19 2015, Seville, 2667-2672. https://doi.org/10.1109/ICIT.2015.7125491

[9] Gunlu, G. (2015) Investigation of Hybrid Fuel Cell-Battery Systems. *ECS Transactions*, **65**, 87-91. https://doi.org/10.1149/06501.0087ecst

[10] Dallinger, D., Krampe, D. and Wietschel, M. (2011) Vehicle-to-Grid Regulation Reserves Based on a Dynamic Simulation of Mobility Behavior. *IEEE Transactions on Smart Grid*, **2**, 302-313. https://doi.org/10.1109/TSG.2011.2131692

[11] Genoese, F. and Genoese, M. (2014) Assessing the Value of Storage in a Future Energy System with a High Share of Renewable Electricity Generation. *Energy Systems*, **5**, 19-44. https://doi.org/10.1007/s12667-013-0076-2

[12] Hoppmann, J., Volland, J., Schmidt, T., Hoffmann, S. and Volker, H. (2014) The Economic Viability of Battery Storage for Residential Solar Photovoltaic Systems—A Review and a Simulation Model. *Renewable and Sustainable Energy Reviews*, **39**, 1101-1118. https://doi.org/10.1016/j.rser.2014.07.068

[13] Betzin, C., Wolfschmidt, H. and Luther, M. (2018) Electrical Operation Behavior and Energy Efficiency of Battery Systems in a Virtual Storage Power Plant for Primary Control Reserve. *International Journal of Electrical Power and Energy Systems*, **97**, 138-145. https://doi.org/10.1016/j.ijepes.2017.10.038

[14] Schlasza, C., Ostertag, P., Chrenko, D., Kriesten, R. and Bouquain, D. (2014) Review on the Aging Mechanisms in Li-Ion Batteries for Electric Vehicles Based on the FMEA Method. *Transportation Electrification Conference and Expo*, Dearborn, June 15-18 2014, 1-6. https://doi.org/10.1109/ITEC.2014.6861811

[15] Vetter, J., Novák, P., Wagner, M.R., Veit, C., Möller, K.-C., Besenhard, J.O., Winter, M., Wohlfahrt-Mehrens, M., Vogler, C. and Hammouche, A. (2015) Ageing Mechanisms in Lithium-Ion Batteries. *Journal of Power Sources*, **14**, 269-281.

[16] Lang, F., Wei, Z., Tan, C.M. and Yazami, R. (2017) Hierachical Degradation Processes in Lithium-Ion Batteries during Ageing, *Electrochimica Acta*, **256**, 52-62. https://doi.org/10.1016/j.electacta.2017.10.007

[17] Kassem, M., Bernard, J., Revel, R., Pélissier, S., Duclaud, F. and Delacourt, C. (2012)

Calendar Aging of a Graphite/$LiFePO_4$ Cell. *Journal of Power Sources*, **208**, 296-305. https://doi.org/10.1016/j.jpowsour.2012.02.068

[18] Käbitz, S., Gerschler, J.B., Ecker, M., Yurdagel, Y., Emmermacher, B., André, D., Mitsch, T. and Sauer, D.U. (2013) Cycle and Calendar Life Study of a Graphite/$LiNi_{1/3}Mn_{1/3}Co_{1/3}O_2$ Li-Ion High Energy System. Part A: Full Cell Characterization. *Journal of Power Sources*, **239**, 572-583. https://doi.org/10.1016/j.jpowsour.2013.03.045

[19] Cho, I.H., Kim, S.S., Shin, S.C. and Choi, N.S. (2010) Effect of SEI on Capacity Losses of Spinel Lithium Manganese Oxide/Graphite Batteries Stored at 60˚C. *Electrochemical and Solid-State Letters*, **13**, A168-A172. https://doi.org/10.1149/1.3481711

[20] Anseán, D., Gonzaléz, M., Viera, J.C., García, V.M., Blacno, C. and Valledor, M. (2013) Fast Charging Technique for High Power Lithium Iron Phosphate Batteries: A Cycle Life Analysis. *Journal of Power Sources*, **239**, 9-15. https://doi.org/10.1016/j.jpowsour.2013.03.044

[21] Bodenes, L., Naturel, R., Martinez, H., Dedryvére, R., Menetrier, M., Croguennec, L., Pérès, J.P., Tessier, C. and Fischer, F. (2013) Lithium Secondary Batteries Working at Very High Temperature: Capacity Fade and Understanding of Aging Mechanisms. *Journal of Power Sources*, **236**, 265-275. https://doi.org/10.1016/j.jpowsour.2013.02.067

[22] Joglekar, M.M. and Ramakrishnan, N. (2013) Cyclic Capacity Fade Plots for Aging Studies of Li-Ion Cells. *Journal of Power Sources*, **230**, 143-147. https://doi.org/10.1016/j.jpowsour.2012.12.060

[23] Barré, A., Deguilhem, B., Grolleau, S., Gérard, M., Suard, F. and Ríu, D. (2013) A Review on Lithium-Ion Battery Ageing Mechanisms and Estimations for Automotive Applications. *Journal of Power Sources*, **241**, 680-689. https://doi.org/10.1016/j.jpowsour.2013.05.040

[24] Liu, P., Wang, J., Hicks-Garner, J., Sherman, E., Soukiazian, S., Verbrugge, M., Tataria, H., Musser, J. and Finamore, P. (2010) Aging Mechanisms of $LiFePO_4$ Batteries Deduced by Electrochemical and Strucutral Analysis. *Journal of the Electrochemical Society*, **157**, A499-A507. https://doi.org/10.1149/1.3246839

[25] Ramana, C.V., Mauger, A., Gendron, F., Julien, C.M. and Zaghib, K. (2009) Study of the Li-Insertion/Extraction Process in $LiFePO_4/FePO_4$. *Journal of Power Sources*, **187**, 555-564. https://doi.org/10.1016/j.jpowsour.2008.11.042

[26] Tarascon, J.M., Mckinnon, W.R., Coowar, F., Bowmer, T.N., Amatucci, G. and Guyomard, D. (1994) Synthesis Conditions and Oxygen Stoichiometry Effects on Li Insertion into the Spinel $LiMn_2O_4$. *Journal of the Electrochemical Society*, **141**, 1421-1431. https://doi.org/10.1149/1.2054941

[27] Gabrisch, H., Tanghong, Y. and Yazami, R. (2008) Transmission Electron Microscope Studies of $LiNi_{1/3}Mn_{1/3}Co_{1/3}O_2$ before and after Long-Term Aging at 70˚C. *Electrochemical and Solid-State Letters*, **11**, A119-A124. https://doi.org/10.1149/1.2919713

[28] Liu, W., Delacourt, C., Forgez, C. and Pelissier, S. (2011) Study of Graphite/NCA Li-Ion Cell Degradation during Accelerated Aging Tests—Data Analysis of the Sim Stock Project. *Vehicle Power and Propulsion*, Chicago, 6-9 September 2011, 1-6. https://doi.org/10.1109/VPPC.2011.6043110

[29] Kubiak, P., Wolfahrt-Mehrens, M., Edstörm, K. and Morcrette, M. (2012) Review on Ageing Mechanisms of Different Li-Ion Batteries for Automotive Applications. Helios Project.

[30] Watanabe, S., Kinoshita, M., Hosokawa, T., Morigaki, K. and Nakura, K. (2014) Capacity Fading of $LiAl_yNi_{1-x-y}Co_xO_2$ Cathode for Lithium-Ion Batteries during Accelerated Calendar and Cycle Life Tests (Effect of Depth of Discharge in Charge Discharge Cycling on the Suppression of the Micro-Crack Generation of $LiAl_yNi_{1-x-y}Co_xO_2$ Particle). *Journal of Power Sources*, **260**, 50-56. https://doi.org/10.1016/j.jpowsour.2014.02.103

[31] Muto, S., Sasano, Y., Tatsumi, K., Sasaki, T., Horibuchi, K., Takeuchi, Y. and Ukyo, Y. (2009) Capacity-Fading Mechanisms of $LiNiO_2$-Based Lithium-Ion Batteries II. Diagnostic Analysis by Electron Microscopy and Spectroscopy. *Journal of the Electrochemical Society*, **156**, A371-A377. https://doi.org/10.1149/1.3076137

[32] Yang, X., Sun, X. and McBreen, J. (1999) New Findings on the Phase Transitions in $Li_{1-x}NiO_2$: *In Situ* Synchrotron X-Ray Diffraction Studies. *Electrochemistry Communications*, **1**, 227-232. https://doi.org/10.1016/S1388-2481(99)00046-6

[33] Atkins, P.W. and Paula, J.D. (2014) Physical Chemistry. Oxford University Press, Oxford, 10th Edition, 920-926.

[34] Macdonald, D.D., Varma, R. and Selman, J.R. (1991) Techniques for Characterization of Electrodes and Electrochemical Processes. Wiley, New York.

[35] Hamann, C.H. and Vielstich, W. (2005) Elektrochemie. Wiley-VCH, Weinheim, 4th Edition, 284-295.

[36] Bard, A.J. and Faulkner, L.R. (2001) Electrochemical Methods. John Wiley & Sons, New York, 2nd Edition, 226-256.

[37] Betzin, C., Wolfschmidt, H. and Luther, M. (2016) Long Time Behavior of $LiNi_{0.80}Co_{0.15}Al_{0.05}O_2$ Based Lithium-Ion Cells by Small Depth of Discharge at Specific State of Charge for Primary Control Reserve in a Virtual Energy Storage Plant. *Energy Procedia*, **99**, 235-242. https://doi.org/10.1016/j.egypro.2016.10.114

[38] Wong, D., Shrestha, D., Wetz, D.A. and Heinzel, J.M. (2015) Impact of High Rate Discharge on the Aging of Lithium Nickel Cobalt Aluminum Oxide Batteries. *Journal of Power Sources*, **280**, 363-372. https://doi.org/10.1016/j.jpowsour.2015.01.110

[39] Barsoukov, E. and Macdonald, J.R. (2005) Impedance Spectroscopy Theory, Experiment and Applications. Wiley, New York. https://doi.org/10.1002/0471716243

[40] Schindler, S., Bauer, M., Petzl, M., Danzer, M. and Michael, A. (2016) Voltage Relaxation and Impedance Spectroscopy as In-Operando Methods for the Detection of Lithium Plating on Graphitic Anodes in Commercial Lithium-Ion Cells. *Journal of Power Sources*, **304**, 170-180. https://doi.org/10.1016/j.jpowsour.2015.11.044

[41] Amemiya, T., Hashimoto, K. and Fujishima, A. (1993) Faradaic Charge Transfer with Double-Layer Charging and/or Adsorption-Related Charging at Polymer-Modified Electrodes as Observed by Color Impedance Spectroscopy. *The Journal of Physical Chemistry*, **97**, 9736-9740. https://doi.org/10.1021/j100140a033

[42] Stroe, D.-I., Swiercynski, M., Stroe, A.-I., Kaer, S.K. and Teodorescu, R. (2017) Lithium-Ion Battery Power Degradation Modelling by Electrochemical Impedance Spectroscopy. *IET Renewable Power Generation*, **11**, 1136-1141. https://doi.org/10.1049/iet-rpg.2016.0958

[43] Stroe, D.-I., Swierczynski, M., Stroe, A.-I., Knap, V., Teodorescu, R. and Andreasen, S.J. (2015) Evaluation of Different Methods for Measuring the Impedance of Lithium-Ion Batteries during Ageing. 10*th International Conference on Ecological Vehicles and Renewable Energies*, Monte Carlo, March 31-April 2 2015, 1-8.

[44] Schönleber, M., Uhlmann, C., Braun, P., Weber, A. and Ivers-Tiffée, E. (2017) A Consistent Derivation of the Impedance of a Lithium-Ion Battery Electrode and Its Dependency on the State-of-Charge. *Electrochimica Acta*, **243**, 250-259.

https://doi.org/10.1016/j.electacta.2017.05.009

[45] Wang, Q. (2017) Ionic Transport and Dielectric Properties in NaNbO under High Pressure. *Applied Physics Letters*, **111**, 152903-152907. https://doi.org/10.1063/1.4999206

[46] Sivakkumar, S.R., Nerkar, J.Y. and Pandolfo, A.G. (2010) Rate Capability of Graphite Materials as Negative Electrodes in Lithium-Ion Capacitors. *Electrochimica Acta*, **55**, 3330-3335. https://doi.org/10.1016/j.electacta.2010.01.059

[47] Abraham, D.P., Kawauchi, S. and Dees, D.W. (2008) Modeling the Impedance Versus Voltage Characteristics of $LiNi_{0.8}Co_{0.15}Al_{0.05}O_2$. *Electrochimica Acta*, **53**, 2121-2129. https://doi.org/10.1016/j.electacta.2007.09.018

[48] Kleiner, K., Dixon, D., Jakes, P., Melke, J., Yavuz, M., Roth, C., Nikolowski, K., Liebau, V. and Ehrenberg, H. (2015) Fatigue of $LiNi_{0.8}Co_{0.15}Al_{0.05}O_2$ in Commercial Li Ion Batteries. *Journal of Power Sources*, **273**, 70-82. https://doi.org/10.1016/j.jpowsour.2014.08.133

[49] Williford, R.E., Viswanathan, V.V. and Zhang, J.-G. (2009) Effects of Entropy Changes in Anodes and Cathodes on the Thermal Behavior of Lithium Ion Batteries. *Journal of Power Sources*, **189**, 101-107. https://doi.org/10.1016/j.jpowsour.2008.10.078

[50] Smith, K. and Wang, C.Y. (2006) Solid-State Diffusion Limitations on Pulse Operation of a Lithium Ion Cell for Hybrid Electric Vehicles. *Journal of Power Sources*, **161**, 628-639. https://doi.org/10.1016/j.jpowsour.2006.03.050

[51] Schlögel, P. (2013) Chemical Energy Storage. De Gruyter Graduate, Berlin, 135-150.

[52] Wu, B., Yufit, V., Merla, Y., Martinez-Botas, R.F., Brandon, N.P. and Offer, G.J. (2015) Differential Thermal Voltammetry for Tracking of Degradation in Lithium-Ion Batteries. *Journal of Power Sources*, **273**, 495-501. https://doi.org/10.1016/j.jpowsour.2014.09.127

[53] Legrand, N., Knosp, B., Desprez, P., Lapicque, F. and Raël, S. (2014) Physical Characterization of the Charging Process of a Li-Ion Battery and Prediction of Li Plating by Electrochemical Modeling. *Journal of Power Sources*, **245**, 208-216. https://doi.org/10.1016/j.jpowsour.2013.06.130

[54] Waldmann, T., Kasper, M. and Wohlfahrt-Mehrens, M. (2015) Optimization of Charging Strategy by Prevention of Lithium Deposition on Anodes in High-Energy Lithium-Ion Batteries—Electrochemical Experiments. *Electrochimica Acta*, **178**, 525-532. https://doi.org/10.1016/j.electacta.2015.08.056